

1 **On the barium - oxygen consumption relationship in the Mediterranean Sea: implications**  
2 **for mesopelagic marine snow remineralisation.**

3

4 Stéphanie H.M. Jacquet<sup>1\*</sup>, Dominique Lefèvre<sup>1</sup>, Christian Tamburini<sup>1</sup>, Marc Garel<sup>1</sup>, Frédéric  
5 A.C. Le Moigne<sup>1</sup>, Nagib Bhairy<sup>1</sup>, Sophie Guasco<sup>1</sup>

6

7 <sup>1</sup>Aix Marseille Université, CNRS/INSU, Université de Toulon, IRD, Mediterranean Institute of  
8 Oceanography (MIO), UM 110, 13288 Marseille, France,

9

10 \*Correspondence to: S. Jacquet (*stephanie.jacquet@mio.osupytheas.fr*)

11

12

13 Biogeosciences

14

15

16

17

18 **ABSTRACT**

19 In the ocean, remineralisation rate associated with sinking particles is a crucial variable. Since  
20 the 90's, particulate biogenic barium ( $Ba_{xs}$ ) has been used as an indicator of carbon  
21 remineralization by applying a transfer function relating  $Ba_{xs}$  to  $O_2$  consumption (Dehairs's  
22 transfer function, Southern Ocean-based). Here, we tested its validity in the Mediterranean Sea  
23 (ANTARES / EMSO-LO) for the first time by investigating connections between  $Ba_{xs}$ ,  
24 prokaryotic heterotrophic production (PHP) and oxygen consumption ( $JO_2$ -Opt; optodes  
25 measurement). We show that: (1) higher  $Ba_{xs}$  (409 pM; 100- 500 m) occurs in situations where  
26 integrated PHP ( $PHP_{100/500} = 0.90$ ) is located deeper, (2) higher  $Ba_{xs}$  occurs with increasing  
27  $JO_2$ -Opt, and (3) similar magnitude between  $JO_2$ -Opt ( $3.14 \text{ mmol m}^{-2} \text{ d}^{-1}$ ; 175- 450 m) and  $JO_2$ -  
28 Ba ( $4.59 \text{ mmol m}^{-2} \text{ d}^{-1}$ ; transfer function). Overall,  $Ba_{xs}$ , PHP and  $JO_2$  relationships follow trends  
29 observed earlier in the Southern Ocean. We conclude that such transfer function could apply in  
30 the Mediterranean Sea.

31  
32  
33 **KEY WORDS:** particulate biogenic barium, mesopelagic zone, oxygen consumption,  
34 prokaryotic heterotrophic production, carbon remineralization, Mediterranean Sea

35

## 36 1. INTRODUCTION

37 Ocean ecosystems play a critical role in the Earth's carbon (C) cycle [IPCC, 2014]. The  
38 quantification of their impacts of both present conditions and future predictions remains one of  
39 the greatest challenges in oceanography [Siegel et al., 2016]. In essence, the biological C pump is  
40 termed for the numerous processes involved in maintaining the vertical gradient in dissolved  
41 inorganic C. This includes processes such as organic matter production in surface, its export and  
42 subsequent remineralization. Most of marine snow organic C conversion (i.e. remineralization)  
43 into CO<sub>2</sub> by heterotrophic organisms (i.e. respiration) occurs in the mesopelagic zone (100-1000  
44 m) [Martin et al., 1987; Buesseler and Boyd, 2009]. Globally, the flux of C exported below 1000  
45 m depth is the key determinant of ocean carbon storage capacity [Henson et al., 2011]. However,  
46 there is no consensus on C transfer efficiency estimations from field experiments, leading to an  
47 imbalance of the water column C budget [Giering et al., 2014]. Resolving this imbalance is in the  
48 core of numerous studies in the global ocean, but also regionally, especially in the Mediterranean  
49 Sea (MedSea). Due to limited exchanges with adjacent basin and the existence of an intense  
50 overturning circulation qualitatively resembling the global one (but with shorter time scales), the  
51 MedSea is often considered as a laboratory to observe and understand the impact of transient  
52 climate variability on ecosystems and biogeochemical cycles [Malanotte-Rissoli et al., 2014]. In a  
53 context of climate changes, better constraining C fluxes and the ocean C storage capacity is of  
54 crucial importance.

55 Particulate barium in excess (Ba<sub>xs</sub>, i.e. biogenic Ba from total particulate Ba after correction for  
56 lithogenic Ba) is a geochemical tracer of particulate organic carbon (POC) remineralization in the  
57 mesopelagic layer [Dehairs et al., 1997]. Ba<sub>xs</sub> mostly occurs in the form of barite microcrystals  
58 (BaSO<sub>4</sub>) at these depths. In a global ocean undersaturated with respect to barite, studies report  
59 that Ba<sub>xs</sub> would precipitate inside oversaturated biogenic micro-environments during POC

60 degradation by heterotrophic prokaryotes in the mesopelagic zone, through sulfate and/or barium  
61 enrichment [Bertram and Cowen, 1997]. The first-ever studies on mesopelagic  $Ba_{xs}$  reported  
62 coinciding  $Ba_{xs}$  maxima with depths of dissolved  $O_2$  minimum and  $pCO_2$  maximum [Dehairs et  
63 al., 1987, 1997]. By using an 1D advection-diffusion model applied to  $O_2$  profiles in the Atlantic  
64 sector of the Southern Ocean (ANTX/6 cruise; Shopova et al., 1995), Dehairs et al. [1997]  
65 established an algorithm converting mesopelagic  $Ba_{xs}$  concentration into  $O_2$  consumption rate  
66 ( $JO_2$ ) and organic C remineralized (POC remineralization rate). This transfer function has been  
67 widely used until now [Cardinal et al., 2001, 2005; Dehairs et al., 2008; Jacquet et al., 2008a,  
68 2008b, 2011, 2015]. Yet its validity has never been tested in other oceanic provinces. In the  
69 North Atlantic, Lemaitre et al. [2018] reported a  $Ba_{xs}$  -  $JO_2$  (obtained from apparent oxygen  
70 utilisation divided by the water mass age) relationship not significantly different to that reported  
71 in Dehairs et al. [1997]. Furthermore, significant progresses were made in relating  $Ba_{xs}$ ,  $O_2$   
72 dynamics to prokaryotic heterotrophic activity [Jacquet et al., 2015]. These advancements clearly  
73 show that  $Ba_{xs}$  is closely related with the vertical distribution of prokaryotes heterotrophic  
74 production (PHP) (the rate of change with depth), reflecting the temporal progression of POC  
75 remineralization processes. Also, in a first attempt to test the validity of the Dehairs's transfer  
76 function in other locations, Jacquet et al. [2015] confronted oxygen consumption rates ( $JO_2$ ) from  
77 direct measurements (dark community respiration, DCR) to derived  $JO_2$  from  $Ba_{xs}$  data (using the  
78 transfer function) in the Kerguelen area (Indian sector of the Southern Ocean). We revealed good  
79 convergence of  $JO_2$  rates from these two approaches, further supporting the Dehairs's function to  
80 estimate POC remineralization rates in different biogeochemical settings of the Southern Ocean.

81 Here, we further investigate relationships between the mesopelagic  $Ba_{xs}$  proxy, prokaryotic  
82 activity and oxygen dynamics (Figure 1a) in the northwestern Mediterranean Sea (MedSea), a  
83 different biogeochemical setting to those already studied (see references above). Today,

84 observations of the various components of the MedSea biological C pump provide organic C  
85 remineralization fluxes varying by at least an order of magnitude [Santinelli et al., 2010;  
86 Ramondenc et al., 2016]. Malanotte-Rissoli et al. [2014] reviewing unsolved issues and future  
87 directions for MedSea research highlighted the need to further investigate biogeochemical  
88 processes at intermediate (mesopelagic) and deep layers to reconcile the C budget in the  
89 Mediterranean basin. Previous particulate  $Ba_{xs}$  dataset is very scarce in the NW- MedSea, with in  
90 general very low vertical sampling resolution [Sanchez Vidal et al., 2005] or very restricted  
91 studied areas [Dehairs et al., 1987; Sternberg et al., 2008]. Here we discuss  $Ba_{xs}$ , PHP and  $JO_2$   
92 (from optodes measurement during incubations) at the ANTARES / EMSO-LO observatory site  
93 (Figure 1a, b). We hypothesize that the Dehairs's transfer function converting  $Ba_{xs}$  into POC  
94 remineralization also applies in a different ocean ecosystem functioning from the Southern  
95 Ocean. We suggest that the  $Ba_{xs}$  proxy can be used as routine tracer to estimate local-scale  
96 processes of mesopelagic POC remineralization in the Mediterranean basin.

97

## 98 **2. METHODS**

### 99 **2.1 STUDY SITE**

100 The BATMAN cruise (<https://doi.org/10.17600/16011100>, March 10-16 2016, *R/V* EUROPE)  
101 took place to the ANTARES / EMSO-LO observatory site (42°48'N, 6°10'E; Tamburini et al.,  
102 2013), 40 km off the coast of Toulon, southern France (Figure 1b). The hydrological and  
103 biogeochemical conditions at this site are monitored monthly in the framework of the MOOSE  
104 (Mediterranean Ocean Observing System for the Environment) program and of the EMSO  
105 (European Multidisciplinary Subsea Observatory) observation program. The hydrography  
106 displays the general three-layer MedSea system with surface, intermediate and deep waters  
107 [Hainbucher et al., 2014]. Briefly, the main water masses can be distinguished (see potential

108 temperature – salinity diagram during the BATMAN cruise in Figure 1c): (1) Surface Water  
109 (SW); (2) Winter Intermediate Water (WIW); (3) Levantine Intermediate water (LIW). LIW is  
110 present at intermediate depths (around 400 m at ANTARES) and is characterized by temperature  
111 and a salinity maxima; (4) Mediterranean Deep Water (MDW).

112

## 113 **2.2 SAMPLING AND ANALYSES**

114 For particulate barium, 4 to 7 L of seawater sampled using Niskin bottles were filtered onto 47  
115 mm polycarbonate membranes (0.4  $\mu\text{m}$  porosity) under slight overpressure supplied by filtered  
116 air. Filters were rinsed with few mL of Milli-Q grade water to remove sea salt, dried (50°C) and  
117 stored in Petri dishes. Thirteen depths between surface and 1000 m were sampled by combining  
118 different casts sampled closely in time and space (total of 28 samples) with similar potential  
119 temperature – salinity profiles. No major changes in water mass characteristics occurred over the  
120 3-day sampling period (Figure 1c). In the laboratory, we performed a total digestion of filters  
121 using a concentrated tri-acid (0.5 mL HF / 1.5 mL HNO<sub>3</sub> / HCl 1 mL; all Optima grade) mixture  
122 in closed teflon beakers overnight at 95°C in a clean pressurized room. After evaporation close to  
123 dryness, samples were re-dissolved into 10 mL of HNO<sub>3</sub> 2%. The solutions were analysed for Ba  
124 and other elements of interest (Na and Al) by HR-ICP-MS (High Resolution-Inductively Coupled  
125 Plasma- Mass Spectrometry; ELEMENT XR ThermoFisher). Based on analyses of external  
126 certified reference standards, accuracy and reproducibility were both within  $\pm 5\%$ . Details on  
127 sample processing and analysis are given in Cardinal et al. [2001] and Jacquet et al. [2015]. The  
128 presence of sea-salt was checked by analysing Na and the sea-salt particulate Ba contribution was  
129 found negligible ( $< 0.1\%$  of total Ba). Particulate biogenic barium in excess (hereafter referred to  
130 as Ba<sub>xs</sub>) was calculated as the difference between total Ba and lithogenic Ba using Al as the  
131 lithogenic reference element. The lithogenic Ba concentration was determined using Al

132 concentration and the upper continental crust (UCC) Ba:Al molar ratio [Taylor and Mc.Lennan,  
133 1985]. The biogenic Ba fraction ranged from 51 to 91 % of the total particulate Ba signal (see  
134 section 3.1). The standard uncertainty [Ellison et al., 2000] on Ba<sub>xs</sub> concentration ranges between  
135 5.0 and 5.5%. The term “in excess” is used to indicate that concentrations are larger than the Ba<sub>xs</sub>  
136 background. The background (or residual value) is considered as “preformed” Ba<sub>xs</sub> at zero  
137 oxygen consumption left over after transfer and partial dissolution of Ba<sub>xs</sub> produced during  
138 degradation of previous phytoplankton growth events. The background is set at 130 pM in this  
139 study.

140 Oxygen concentrations were measured using oxygen optode Aanderaa® 4330 for at least 24  
141 hours (on a 30 seconds time step) on samples taken at 4 depths in the mesopelagic layer (175,  
142 250, 450 and 1000 m). Samples were placed into a sealed 1L borosilicate glass bottles incubated  
143 at a constant temperature of 13°C in thermo-regulated baths. Optodes were calibrated using a  
144 home made calibration facility ([https://www.mio.osupytheas.fr/en/cybele/oxygen-dynamics-  
145 construction-oxygen-optode-calibration-platform](https://www.mio.osupytheas.fr/en/cybele/oxygen-dynamics-construction-oxygen-optode-calibration-platform)). Oxygen consumption rates (later referred to as  
146 JO<sub>2</sub>-Opt) were derived from a linear model calculation. Associated errors to the linear model fit  
147 are below 0.01 μM O<sub>2</sub> h<sup>-1</sup>. Each oxygen consumption experiment has been duplicated for each  
148 depth. Average and standard deviation of the duplicates are reported in Fig 3a. The larger  
149 associated errors are related to the differences between each duplicates, especially in surface,  
150 reflecting potential heterogeneity of the microbial community during sampling.

151 Prokaryotic heterotrophic production (PHP) estimation was measured over time course  
152 experiments at *in situ* temperature (13°C) following the protocol described in Tamburini et al.  
153 [2002]. <sup>3</sup>H-leucine labelled tracer [Kirchman, 1993] was used. To calculate prokaryotic  
154 heterotrophic production, we used the empirical conversion factor of 1.55 ng C per pmol of

155 incorporated leucine according to Simon and Azam [1989], assuming that isotope dilution was  
156 negligible under these saturating concentrations.

157

### 158 **3. RESULTS AND DISCUSSION**

#### 159 **3.1 Particulate Ba<sub>xs</sub> vertical distribution**

160 Particulate biogenic Ba<sub>xs</sub>, particulate Al (pAl) and biogenic Ba fraction profiles in the upper  
161 1000 m at ANTARES are reported in Figure 2a. Ba<sub>xs</sub> concentrations range from 12 to 719 pM.  
162 The biogenic Ba fraction ranges from 51 to 91 % of the total particulate Ba signal. Particulate Al  
163 concentrations (pAl) range from 8 to 170 nM. Ba<sub>xs</sub> concentrations are low in surface water (<100  
164 pM) where the lithogenic fraction reaches 43 to 49 % in the upper 70 m. From previous studies  
165 we know that Ba<sub>xs</sub> in surface waters is distributed over different, mainly non-barite biogenic  
166 phases, and incorporated into or adsorbed onto phytoplankton material. As such these do not  
167 reflect POC remineralization processes, in contrast to mesopelagic waters where Ba<sub>xs</sub> is mainly  
168 composed of barite formed during prokaryotic degradation of organic matter. Focus is done in the  
169 present study on the mesopelagic layer. The Ba<sub>xs</sub> profile at ANTARES indeed displays a  
170 mesopelagic Ba<sub>xs</sub> maximum between 100 and 500 m, reaching up to 719 pM at 175 m. Ba is  
171 mostly biogenic at these depths (> 80 %). Ba<sub>xs</sub> concentrations then decrease below 500 m to  
172 reach a background value of around 130 pM (see BKG in Figure 2). Note that the MedSea is  
173 largely undersaturated with respect to barite, with saturation state ranging between 0.2 and 0.6  
174 over the basin [Jacquet et al., 2016; Jullion et al., 2017]. For comparison, the Ba<sub>xs</sub> background  
175 value in the Southern Ocean reaches 180 to 200 pM below 1000 m [Dehairs et al., 1997; Jacquet  
176 et al. 2015]. Previously, Sternberg et al. [2008] reported the seasonal evolution of Ba<sub>xs</sub> profiles at  
177 the DYFAMED station (43°25'N-7°52'E; BARMED project) northeast from ANTARES (Figure  
178 1c) in the NW-MedSea. The present Ba<sub>xs</sub> profile at ANTARES (March 2016) is very similar to



179 the  $Ba_{xs}$  profile measured in March 2003 at DYFAMED (Figure 2a). The slight difference  
180 between  $Ba_{xs}$  profiles in the upper 75 m suggests more Ba bounded and/or adsorbed onto  
181 phytoplankton material during BARMED. Both profiles present a  $Ba_{xs}$  maximum in the upper  
182 mesopelagic zone between 150 and 200 m. Below this maximum,  $Ba_{xs}$  concentrations gradually  
183 decrease to reach around 130 pM between 500 and 1000 m (this study). A similar value was  
184 reached between 500 and 600 m at the DYFAMED station over the whole studied period  
185 (between February and June 2003; Sternberg et al., 2008).

186

### 187 **3.2 Prokaryotic heterotrophic production**

188 The particulate Ba in excess is centred in the upper mesopelagic zone between 100 and 500 m  
189 and reflects that POC remineralization mainly occurred at this depth layer (Figure 2a). Depth-  
190 weighted average (DWA)  $Ba_{xs}$  content (409 pM), i.e. the  $Ba_{xs}$  inventory divided by the depth  
191 layer considered, was calculated between 100 and 500 m. Figure 2b shows the column-integrated  
192 PHP at 100 m over the one at 500 m (PHP100/500). Our PHP100/500 ratio at ANTARES station  
193 is of 0.90 and is compared to results obtained during KEOPS1 (summer) and KEOPS2 (spring;  
194 out plateau stations) cruises in the Southern Ocean [Jacquet et al., 2008; 2015] and #DY032  
195 cruise (July 2015, *R/V DISCOVERY*) at the PAP (Porcupine Abyssal Plain) observatory in the  
196 northeast Atlantic (49°N, 16.5 °W) (personal data). Result at the ANTARES / EMSO-LO site  
197 follows the trend previously reported in the Southern Ocean (blue line in Figure 2b; Jacquet et al.,  
198 2015), indicating higher DWA  $Ba_{xs}$  in situations where a significant part of column-integrated  
199 PHP is located deeper in the water column (high Int. PHPx1/IntPHPx2 ratio; Figure 2b). These  
200 previous studies revealed that the shape of the column-integrated PHP profile (i.e. the attenuation  
201 gradient) is important in setting the  $Ba_{xs}$  signal in the mesopelagic zone (Dehairs et al., 2008;  
202 Jacquet et al., 2008, 2015]. Indeed, mesopelagic DWA  $Ba_{xs}$  appears reduced when most of the

203 column-integrated PHP is limited to the upper layer, i.e. indicating an efficient remineralization  
204 in surface. In contrast, mesopelagic DWA  $Ba_{xs}$  appears higher when most of the column-  
205 integrated PHP is located in the mesopelagic layer, i.e. reflecting significant deep PHP activity,  
206 POC export and subsequent remineralization (Figure 2b). Results at the PAP site reflect a similar  
207 situation as observed during KEOPS2 for time series stations at Plateau site and in a meander of  
208 the polar front area (not show in Figure 2b). At these stations, Jacquet et al. [2015] reported a  
209 shift toward the KEOPS1 trend reflecting the temporal evolution (season advancement) and  
210 patchiness of the establishment of mesopelagic remineralization processes within a same area.  
211 Overall, our MedSea result is located along the trend defined in the Southern Ocean during  
212 KEOPS1 cruise. It is generally considered that  $Ba_{xs}$  (barite) forms inside sulfate and/or barium  
213 oversaturated biogenic micro-environments during POC degradation by heterotrophic  
214 prokaryotes. However, it is unclear whether barite formation at mesopelagic depths is (directly or  
215 indirectly) bacterially induced or bacterially influenced [Martinez-Ruiz et al., 2018, 2019]. In any  
216 case our results strengthen the close link between the water column  $Ba_{xs}$  distribution and  
217 respiration (organic matter degradation).

218

### 219 **3.3 Oxygen- barium relationship**

220 The relationship we obtained at ANTARES between  $Ba_{xs}$  concentrations and oxygen  
221 consumption rates from optodes measurements ( $JO_2$ -Opt) is reported in Figure 3a.  $JO_2$ -Opt range  
222 from 0.11 to 5.85  $\mu\text{mol L}^{-1} \text{d}^{-1}$ . The relationship indicates higher  $Ba_{xs}$  concentrations with  
223 increasing  $JO_2$ -Opt. An interesting feature is the intercept at zero  $JO_2$ -Opt (around 128 pM)  
224 which further supports the Ba BKG value at ANTARES (130 pM) determined from measured  
225  $Ba_{xs}$  profiles (Figure 3a).

226 In figure 3b we applied a similar approach as reported in Jacquet et al. [2015] where we show  
227 the correlation between  $JO_2$  obtained from dark community respiration DCR (Winkler titration;  
228  $JO_2$ -DCR) data integration in the water column and  $JO_2$  based on  $Ba_{xs}$  content (Dehairs's transfer  
229 function; later referred to as  $JO_2$ -Ba). Similarly, to estimate  $JO_2$ -Ba in the present study we used  
230 the following equation [Dehairs et al., 1997] (Figure 3c):

$$231 \quad JO_2\text{-Ba} = (Ba_{xs} - Ba \text{ BKG}) / 17450 \quad (1)$$

232 A Ba BKG value of 130 pM was used (see above).  $JO_2$ -Ba is confronted to  $JO_2$ -Opt integrated  
233 over the same layer depth (between 175 and 450 m; Figure 3b).  $JO_2$  rates are of the same order of  
234 magnitude ( $JO_2$ -Ba = 4.59 mmol m<sup>-2</sup> d<sup>-1</sup> and  $JO_2$ -opt = 3.14 mmol m<sup>-2</sup> d<sup>-1</sup>). The slight difference  
235 could be explained by the integration time of both methods: few hours to days for the incubations  
236 vs. few days to weeks for  $Ba_{xs}$  (seasonal build-up; Jacquet et al., 2007).  $JO_2$  rates calculated in the  
237 present work are 3 times higher than those reported in the Southern Ocean during KEOPS1  
238 [Jacquet et al., 2015] but they are in good agreement with the  $Ba_{xs}$  vs  $JO_2$  trend (Figure 3b).  
239 DWA  $Ba_{xs}$  and  $JO_2$  measured during KEOPS1 [Jacquet et al., 2015] and at ANTARES site (this  
240 study) are compared to Dehairs's relationship in Figure 3c. The correlation obtained in Lemaitre  
241 et al. [2018] in the North Atlantic is also reported ( $JO_2$  were calculated from apparent oxygen  
242 utilisation divided by water mass age). Note that this relationship is not significantly different  
243 from the Dehairs's equation [Lemaitre et al., 2018]. Overall, results at the ANTARES site are  
244 lying along the Southern Ocean  $Ba_{xs}$  -  $JO_2$  correlation. This further supports the validity of the  
245 Dehairs's transfer function in the present study.

246

### 247 **3.4 Estimated particles remineralisation rates and implications**

248 In order to provide a  $Ba_{xs}$ -derived estimate of POC remineralization rate (MR) at the  
249 ANTARES / EMSO-LO observatory during BATMAN cruise, we converted  $JO_2$ -Ba into C

250 respired using the Redfield (RR) C/O<sub>2</sub> molar ratio (127/175; Broecker et al., 1985) multiplied by  
251 the depth layer considered (Z, 175-450 m) [Dehairs et al., 1997]:

$$252 \quad MR = Z \times JO_2\text{-Ba} \times RR \quad (2)$$

253 We obtain a POC remineralization rate of 11 mmol C m<sup>-2</sup> d<sup>-1</sup> (10% RSD). This is within the  
254 range of dissolved Ba- derived fluxes of POC remineralization (13 to 29 mmol C m<sup>-2</sup> d<sup>-1</sup>)  
255 reported in the Mediterranean Sea previously [Jacquet et al., 2016; Jullion et al., 2017].  
256 Following calculations reported in Jullion et al. [2007], our MR rate would correspond to a Ba<sub>xs</sub>  
257 flux of around 0.01 μmol m<sup>-2</sup> d<sup>-1</sup>. This is in reasonable agreement with barium fluxes (0.01 to  
258 0.08 μmol m<sup>-2</sup> d<sup>-1</sup>) presented in Jullion et al. [2007]. Previously published barium fluxes from  
259 sediment trap range from 0.27 to 0.36 μmol m<sup>-2</sup> d<sup>-1</sup> at the DYFAMED station [Sternberg et al.,  
260 2007] and from 0.39 to 1.07 μmol m<sup>-2</sup> d<sup>-1</sup> in the Alboran Sea [Sanchez-Vidal et al., 2005]. POC  
261 remineralization rate from the present study is in the range of previously published carbon export  
262 fluxes (few to tens mmol m<sup>-2</sup> d<sup>-1</sup>) from thorium-derived data [Speicher et al., 2006] or from  
263 combining drifting sediment traps and underwater vision profilers [Ramondenc et al., 2016].  
264 Constraining POC flux attenuation and remineralization rates in the Mediterranean is far from  
265 being achieved, especially regarding seasonal changes and inter-basin variations, but the  
266 concordance of the different approaches is promising.

267

#### 268 4. CONCLUSIONS

269 The present paper brings a first insight into the connections of Ba<sub>xs</sub>, PHP and JO<sub>2</sub> at the  
270 ANTARES/EMSO-LO observatory site in the northwestern Mediterranean Sea during the  
271 BATMAN (2016) cruise. Our results reveal a strong relationship between Ba<sub>xs</sub> contents and  
272 measured JO<sub>2</sub> rates. Also, DWA Ba<sub>xs</sub> vs. column integrated PHP, as well as measured vs. Ba<sub>xs</sub>-  
273 based JO<sub>2</sub> relationships follow trends previously reported in the Southern Ocean where the

274 Dehairs's function was first established to estimate POC remineralisation rate. Results from the  
275 present study would indicate that this function can also be applied in the Mediterranean basin  
276 provided that adequate  $Ba_{xs}$  background values are estimated. From a global climate perspective,  
277 the  $Ba_{xs}$  tool will help to better balance the MedSea water column C budget. It will contribute to  
278 gain focus on the emerging picture of the C transfer efficiency (strength of the biological pump).

279

## 280 **DATA AVAILABILITY**

281 All data and metadata will be made available at the French INSU/CNRS LEFE CYBER  
282 database (scientific coordinator: Hervé Claustre; data manager, webmaster: Catherine  
283 Schmechtig). INSU/CNRSLEFE CYBER (2020)

284

## 285 **AUTHOR CONTRIBUTION**

286 SJ and DL designed the experiment for  $JO_2$ . SJ, CT and MG designed the experiments for PHP  
287 measurements. SJ and FLM managed barium sampling during the cruise. NB managed CTD  
288 deployment at sea. MG, SG and MR managed PHP. All co-authors contributed to writing.

289

## 290 **COMPETING INTERESTS**

291 The authors declare that they have no known competing financial interests or personal  
292 relationships that could have appeared to influence the work reported in this paper.

293

## 294 **ACKNOWLEDGEMENTS**

295 We thank the officers and crew of *R/V EUROPE* for their assistance during work at sea. This  
296 research was supported by the French national LEFE/INSU "REPAP" project (PI. S. Jacquet). It  
297 was co-funded by the "ROBIN" project (PIs. C. Tamburini, F.A.C. Le Moigne) of Labex OT-  
298 Med (ANR-11-LABEX-0061) funded by the Investissements d'Avenir and the French  
299 Government project of the ANR, through the A\*Midex project (ANR-11-IDEX-0001-02).

300 Authors have benefited of the support of the SNO-MOOSE and SAM-MIO. BATMAN is a

301 contribution to the "AT – POMPE BIOLOGIQUE" of the Mediterranean Institute of  
302 Oceanography (MIO) and to the international IMBER program. The instrument (ELEMENT XR,  
303 ThermoFisher) was supported in 2012 by European Regional Development Fund (ERDF).

304

305 **Figure captions**

306 Figure 1: (a) Schematic representation of the convergence of the different estimators of oxygen  
307 consumption and C remineralization rates from the “oxygen dynamics”, “barium proxy” and  
308 “prokaryotic activity” tools; (b) Location of the BATMAN cruise at the ANTARES observatory  
309 site in the NW-Mediterranean Sea (42°48’N, 6°10’E). The location of the DYFAMED station is  
310 reported for comparison (Sternberg et al., 2008); (c) Potential temperature - salinity - depth plots  
311 and isopycals for BATMAN profiles. SW : Surface Water, WIW : Winter Intermediate Water,  
312 LIW : Levantine Intermediate Water, DMW : Deep Mediterranean Water. Graph constructed  
313 using Ocean Data View (Schlitzer, 2002; Ocean Data View; [http://www.awi-  
315 bremerhaven.de/GEO/ODV](http://www.awi-<br/>314 bremerhaven.de/GEO/ODV))

316 Figure 2: (a) Particulate biogenic  $Ba_{xs}$  (pM) and particulate Al (nM) profiles next to the biogenic  
317 Ba fraction (%) in the upper 1000 m at ANTARES. The grey area represents a biogenic Ba  
318 fraction larger than 80 %. BKG:  $Ba_{xs}$  background.  $Ba_{xs}$  profile (pM) at DYFAMED : data from  
319 Sternberg et al. (2008); (b) ANTARES ratio plot (green square) of integrated PHP in the upper  
320 100 m over integrated PHP in the upper 500 m versus depth-weighted average (DWA)  
321 mesopelagic  $Ba_{xs}$  (pM) over the 100-500m depth interval. Regression of the same ratio is  
322 reported for KEOPS1 (light blue symbols; out plateau stations) and KEOPS2 (dark blue symbols;  
323 Southern Ocean, Jacquet et al., 2015) and #DY032 (red square; PAP station, NE-Atlantic; pers.  
324 data) cruises. The blue line represents the trend obtained during KEOPS2 (Jacquet et al., 2015).

325  
326 Figure 3: (a) Relationship between  $Ba_{xs}$  concentrations (pM) and oxygen consumption rates  
327 ( $\mu\text{mol L}^{-1} \text{d}^{-1}$ ) from optodes measurements ( $\text{JO}_2\text{-Opt}$ ) at ANTARES; (b) Confrontation of oxygen  
328 consumption rates ( $\text{JO}_2$ ;  $\text{mmol m}^{-2} \text{d}^{-1}$ ) obtained from different methods: optodes measurements

329 (this study; green square) and dark community respiration DCR (winkler titration; red triangles;  
330  $\text{JO}_2$ -DCR; Jacquet et al., 2015; KEOPS1), and Dehairs's transfer function calculation (Dehairs et  
331 al., 1997) based on  $\text{Ba}_{\text{xs}}$  contents. The black line corresponds to the correlation obtained during  
332 KEOPS1 (Jacquet et al., 2015); (c) Dehairs's relationship between depth-weighted average  
333 (DWA) mesopelagic  $\text{Ba}_{\text{xs}}$  (pM) and  $\text{JO}_2$  ( $\mu\text{mol L}^{-1} \text{d}^{-1}$ ) compared to ANTARES result (this  
334 study), KEOPS1 data (Southern Ocean; Jacquet et al., 2015) and GEOVIDE correlation (North  
335 Atlantic; Lemaitre et al., 2018).

336



337 **References**

- 338 Bertram, Miriam, and James P. Cowen. “Morphological and Compositional Evidence for Biotic  
339 Precipitation of Marine Barite.” *Journal of Marine Research* 55 (1997): 577–93.
- 340 Broecker, Wallace S. “‘NO’, a Conservative Water-Mass Tracer.” *Earth and Planetary Science*  
341 *Letters* 23, no. 1 (August 1974): 100–107. doi:10.1016/0012-821X(74)90036-3.
- 342 Buesseler, Ken O., and Philip W. Boyd. “Shedding Light on Processes That Control Particle  
343 Export and Flux Attenuation in the Twilight Zone of the Open Ocean.” *Limnology and*  
344 *Oceanography* 54, no. 4 (2009): 1210–32. doi:10.4319/lo.2009.54.4.1210.
- 345 Cardinal, Damien, Frank Dehairs, Thierry Cattaldo, and Luc André. “Geochemistry of Suspended  
346 Particles in the Subantarctic and Polar Frontal Zones South of Australia: Constraints on  
347 Export and Advection Processes.” *Journal of Geophysical Research: Oceans* 106, no. C12  
348 (décembre 2001): 31637–56. doi:10.1029/2000JC000251.
- 349 **Cardinal D.**, Savoye N., Trull T. W., André L., Kopczynska E. E., and Dehairs F.: Variations of  
350 carbon remineralisation in the Southern Ocean illustrated by the Baxs proxy, *Deep-Sea Res.*  
351 Pt. I, 52, 355–370, <https://doi.org/10.1016/j.dsr.2004.10.002>, 2005.
- 352 Dehairs, F., R. Chesselet, and J. Jedwab. “Discrete Suspended Particles of Barite and the Barium  
353 Cycle in the Open Ocean.” *Earth and Planetary Science Letters* 49, no. 2 (September 1980):  
354 528–50. doi:10.1016/0012-821X(80)90094-1.
- 355 Dehairs, F., S. Jacquet, N. Savoye, B. A. S. Van Mooy, K. O. Buesseler, J. K. B. Bishop, C. H.  
356 Lamborg, et al. “Barium in Twilight Zone Suspended Matter as a Potential Proxy for

357 Particulate Organic Carbon Remineralization: Results for the North Pacific.” *Deep Sea*  
358 *Research Part II: Topical Studies in Oceanography*, Understanding the Ocean’s Biological  
359 Pump:results from VERTIGO, 55, no. 14–15 (juillet 2008): 1673–83.  
360 doi:10.1016/j.dsr2.2008.04.020.

361 Dehairs, F., C. E. Lambert, R. Chesselet, and N. Risler. “The Biological Production of Marine  
362 Suspended Barite and the Barium Cycle in the Western Mediterranean Sea.”  
363 *Biogeochemistry* 4, no. 2 (June 1, 1987): 119–40. doi:10.1007/BF02180151.

364 Dehairs, F., D. Shopova, S. Ober, C. Veth, and L. Goeyens. “Particulate Barium Stocks and  
365 Oxygen Consumption in the Southern Ocean Mesopelagic Water Column during Spring and  
366 Early Summer: Relationship with Export Production.” *Deep Sea Research Part II: Topical*  
367 *Studies in Oceanography* 44, no. 1–2 (1997): 497–516. doi:10.1016/S0967-0645(96)00072-  
368 0.

369 Ellison, Eurachem/CITAC Guide CG4, Quantifying Uncertainty in Analytical Measurement.  
370 Eds. S.L.R. Ellison, M. Rosslein and A. Williams. Second edition ISBN 0948926 15 5, Pp  
371 120, 2000.

372 Giering, Sarah L. C., Richard Sanders, Richard S. Lampitt, Thomas R. Anderson, Christian Tamburini,  
373 Mehdi Boutrif, Mikhail V. Zubkov, et al. “Reconciliation of the Carbon Budget in the Ocean’s  
374 Twilight Zone.” *Nature* 507, no. 7493 (March 27, 2014): 480–83.

375 Hainbucher, D., A. Rubino, V. Cardin, T. Tanhua, K. Schroeder, and M. Bensi. “Hydrographic  
376 Situation during Cruise M84/3 and P414 (spring 2011) in the Mediterranean Sea.” *Ocean*  
377 *Sci.* 10, no. 4 (juillet 2014): 669–82. doi:10.5194/os-10-669-2014.

378 Henson, Stephanie A., Richard Sanders, Esben Madsen, Paul J. Morris, Frédéric Le Moigne, and  
379 Graham D. Quartly. “A Reduced Estimate of the Strength of the Ocean’s Biological Carbon  
380 Pump.” *Geophysical Research Letters* 38, no. 4 (février 2011): L04606.  
381 doi:10.1029/2011GL046735.

382 IPCC Working Group 1, 5<sup>th</sup> Assessment Report (AR5) Climate Change 2013, Published in Jan.  
383 2014.

384 **Jacquet S.H.M., Dehairs F., Dumont I., Becquevort S., Cavagna A.-J., Cardinal, D.:** Twilight  
385 zone organic carbon remineralization in the Polar Front Zone and Subantarctic Zone south  
386 of Tasmania, *Deep-Sea Res. Pt. II*, 58, 2222–2234, <https://doi.org/10.1016/j.dsr2.2011.05.029>,  
387 **2011.**

388 Jacquet, S. H. M., F. Dehairs, D. Lefèvre, A. J. Cavagna, F. Planchon, U. Christaki, L. Monin, L.  
389 André, I. Closset, and D. Cardinal. “Early Spring Mesopelagic Carbon Remineralization and  
390 Transfer Efficiency in the Naturally Iron-Fertilized Kerguelen Area.” *Biogeosciences* 12, no.  
391 6 (March 17, 2015): 1713–31. doi:10.5194/bg-12-1713-2015.

392 Jacquet, S. H. M., F. Dehairs, N. Savoye, I. Obernosterer, U. Christaki, C. Monnin, and D.  
393 Cardinal. “Mesopelagic Organic Carbon Remineralization in the Kerguelen Plateau Region  
394 Tracked by Biogenic Particulate Ba.” *Deep Sea Research Part II: Topical Studies in*  
395 *Oceanography*, KEOPS: Kerguelen Ocean and Plateau compared Study, 55, no. 5–7 (March  
396 2008): 868–79. doi:10.1016/j.dsr2.2007.12.038, 2008b

397 Jacquet, S. H. M., J. Henjes, F. Dehairs, A. Worobiec, N. Savoye, and D. Cardinal. “Particulate  
398 Ba-Barite and Acantharians in the Southern Ocean during the European Iron Fertilization

399 Experiment (EIFEX).” *Journal of Geophysical Research* 112, no. G4 (October 23, 2007).  
400 doi:10.1029/2006JG000394.

401 Jacquet, S.H.M., C. Monnin, V. Riou, L. Jullion, and T. Tanhua. “A High Resolution and Quasi-  
402 Zonal Transect of Dissolved Ba in the Mediterranean Sea.” *Marine Chemistry* 178 (January  
403 20, 2016): 1–7. doi:10.1016/j.marchem.2015.12.001.

404 **Jacquet** S.H.M., Savoye N., Dehairs F., Strass V.H., Cardinal D.: Mesopelagic carbon remineralization  
405 during the European Iron Fertilization Experiment, *Global Biogeochem. Cy.*, 22, 1–9,  
406 <https://doi.org/10.1029/2006GB002902>, **2008a**.

407 Jullion, L., S. H. M. Jacquet, and T. Tanhua. “Untangling Biogeochemical Processes from the  
408 Impact of Ocean Circulation: First Insight on the Mediterranean Dissolved Barium  
409 Dynamics.” *Global Biogeochemical Cycles* 31, no. 8 (2017): 1256–70.  
410 doi:10.1002/2016GB005489.

411 Kirchman DL (1993) Leucine incorporation as a measure of biomass production by heterotrophic  
412 bacteria. In: Kemp PF, Sherr BF, Sherr EB, Cole JJ (eds) *Handbooks of methods in aquatic  
413 microbial ecology*. Lewis Publishers, Boca Raton, Ann Arbor, London, Tokyo, p 509–512

414 Lemaitre, N., H. Planquette, F. Planchon, G. Sarthou, S. Jacquet, M. I. García-Ibáñez, A.  
415 Gourain, et al. “Particulate Barium Tracing of Significant Mesopelagic Carbon  
416 Remineralisation in the North Atlantic.” *Biogeosciences* 15, no. 8 (2018): 2289–2307.  
417 doi:10.5194/bg-15-2289-2018.

418 Malanotte-Rizzoli, P., V. Artale, G. L. Borzelli-Eusebi, S. Brenner, A. Crise, M. Gacic, N. Kress,  
419 et al. “Physical Forcing and Physical/biochemical Variability of the Mediterranean Sea: A

420 Review of Unresolved Issues and Directions for Future Research.” *Ocean Science* 10, no. 3  
421 (2014): 281–322. doi:10.5194/os-10-281-2014.

422 Martin, John H., George A. Knauer, David M. Karl, and William W. Broenkow. “VERTEX:  
423 Carbon Cycling in the Northeast Pacific.” *Deep Sea Research Part A. Oceanographic  
424 Research Papers* 34, no. 2 (1987): 267–85. doi:http://dx.doi.org/10.1016/0198-  
425 0149(87)90086-0.

426 Martinez-Ruiz, Francisca, Fadwa Jroundi, Adina Paytan, Isabel Guerra-Tschuschke, María del  
427 Mar Abad, and María Teresa González-Muñoz. “Barium Bioaccumulation by Bacterial  
428 Biofilms and Implications for Ba Cycling and Use of Ba Proxies.” *Nature Communications*  
429 9, no. 1 (April 24, 2018): 1619. doi:10.1038/s41467-018-04069-z.

430 Martinez-Ruiz, F., A. Paytan, M.T. Gonzalez-Muñoz, F. Jroundi, M.M. Abad, P.J. Lam, J.K.B.  
431 Bishop, T.J. Horner, P.L. Morton, and M. Kastner. “Barite Formation in the Ocean: Origin  
432 of Amorphous and Crystalline Precipitates.” *Chemical Geology* 511 (April 20, 2019): 441–  
433 51. doi:10.1016/j.chemgeo.2018.09.011.

434 Ramondenc, Simon, Goutx Madeleine, Fabien Lombard, Chiara Santinelli, Lars Stemmann,  
435 Gabriel Gorsky, and Lionel Guidi. “An Initial Carbon Export Assessment in the  
436 Mediterranean Sea Based on Drifting Sediment Traps and the Underwater Vision Profiler  
437 Data Sets.” *Deep Sea Research Part I: Oceanographic Research Papers* 117 (November  
438 2016): 107–19. doi:10.1016/j.dsr.2016.08.015.

439 Sanchez-Vidal, A., R. W. Collier, A. Calafat, J. Fabres, and M. Canals (2005), Particulate barium  
440 fluxes on the continental margin: A study from the Alboran Sea (Western Mediterranean),  
441 *Mar. Chem.*, 93, 105–117.

442 Santinelli, Chiara, Luciano Nannicini, and Alfredo Seritti. “DOC Dynamics in the Meso and Bathypelagic  
443 Layers of the Mediterranean Sea.” *Deep Sea Research Part II: Topical Studies in Oceanography*,  
444 Ecological and Biogeochemical Interactions in the Dark Ocean, 57, no. 16 (août 2010): 1446–59.  
445 doi:10.1016/j.dsr2.2010.02.014.

446 Siegel DA, Buesseler KO, Behrenfeld MJ, Benitez-Nelson CR, Boss E, Brzezinski MA, Burd A, Carlson  
447 CA, D'Asaro EA, Doney SC, Perry MJ, Stanley RHR and Steinberg DK (2016) Prediction of the  
448 Export and Fate of Global Ocean Net Primary Production: The EXPORTS Science Plan. *Front. Mar.*  
449 *Sci.* 3:22. doi: 10.3389/fmars.2016.00022

450 Simon M, Azam F (1989) Protein content and protein synthesis rates of planktonic marine  
451 bacteria. *Mar Ecol Prog Ser* 51:201–213

452 Shopova, D., F. Dehairs, and W. Baeyens. “A Simple Model of Biogeochemical Element  
453 Distribution in the Oceanic Water Column.” *Journal of Marine Systems* 6, no. 4 (juin 1995):  
454 331–44. doi:10.1016/0924-7963(94)00032-7.

455 Speicher, E. A., S. B. Moran, A. B. Burd, R. Delfanti, H. Kaberi, R. P. Kelly, C. Papucci, et al.  
456 “Particulate Organic Carbon Export Fluxes and Size-Fractionated POC/234Th Ratios in the  
457 Ligurian, Tyrrhenian and Aegean Seas.” *Deep Sea Research Part I: Oceanographic*  
458 *Research Papers* 53, no. 11 (2006): 1810–30.  
459 doi:http://dx.doi.org/10.1016/j.dsr.2006.08.005.

460 Sternberg, E., C. Jeandel, E. Robin, and M. Souhaut. “Seasonal Cycle of Suspended Barite in the  
461 Mediterranean Sea.” *Geochimica et Cosmochimica Acta* 72, no. 16 (2008): 4020–34.  
462 doi:<https://doi.org/10.1016/j.gca.2008.05.043>.

463 Tamburini C, Canals M, Durieu de Madron X, Houpert L, Lefèvre D, Martini S, D’Ortenzio F,  
464 Robert A, Testor P, and the ANTARES collaboration (2013) Deep-sea bioluminescence  
465 blooms after dense water formation at the ocean surface. *PLoS One* 8:e67523

466 Tamburini C, Garcin J, Ragot M, Bianchi A (2002) Biopolymer hydrolysis and bacterial  
467 production under ambient hydrostatic pressure through a 2000 m water column in the NW  
468 Mediterranean. *Deep Res II* 49:2109–2123

469 Taylor, S.R., McLennan, S.M.: The continental crust: its composition and evolution, Blackwell  
470 Scientific Publications, 312pp, 1985.

471

472

473

474

475

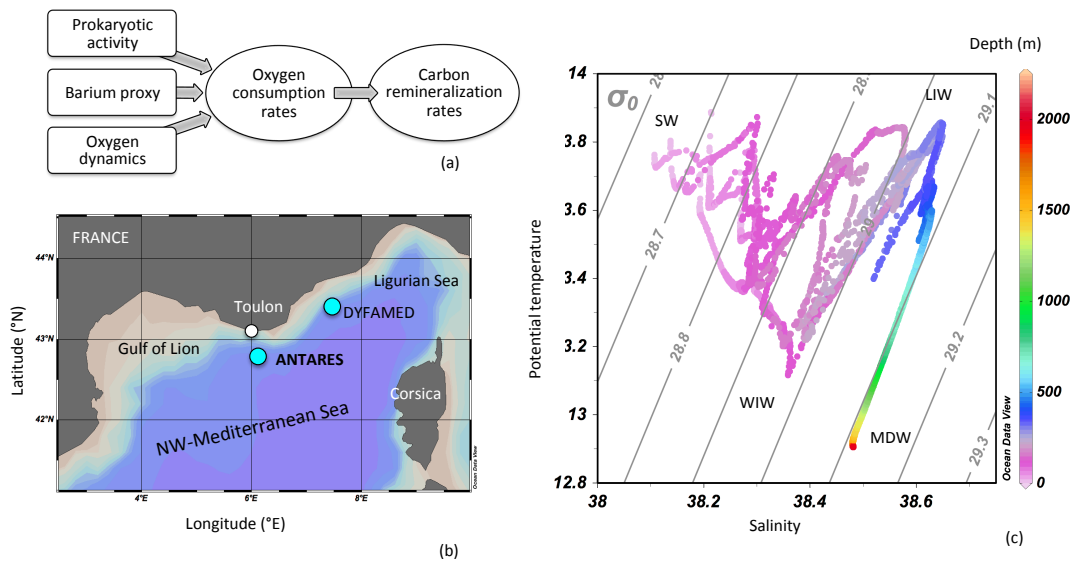
476

477

478

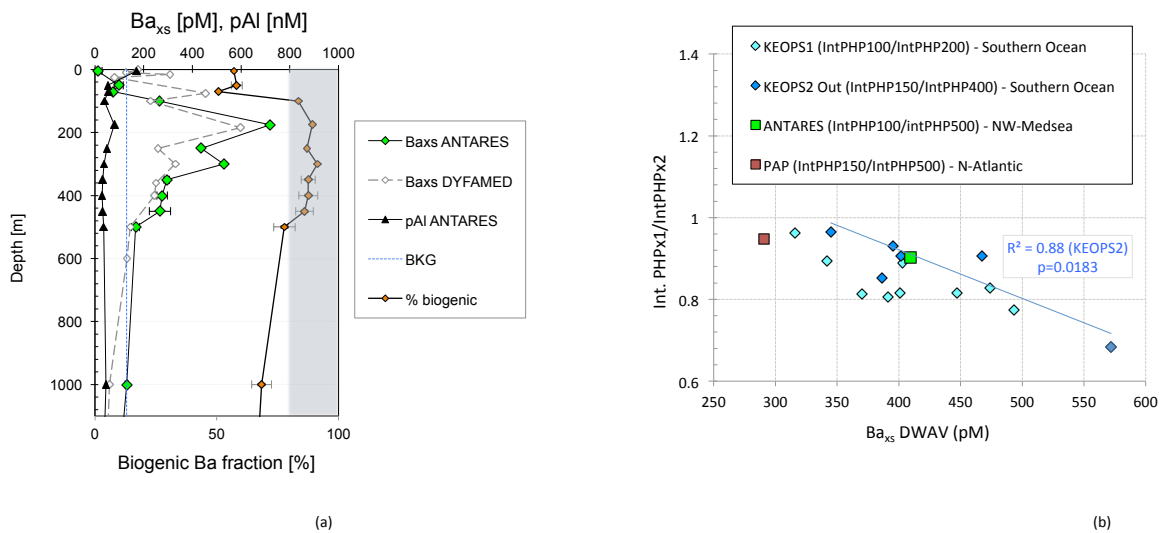
479

480 FIGURE 1



481

482 FIGURE 2



483

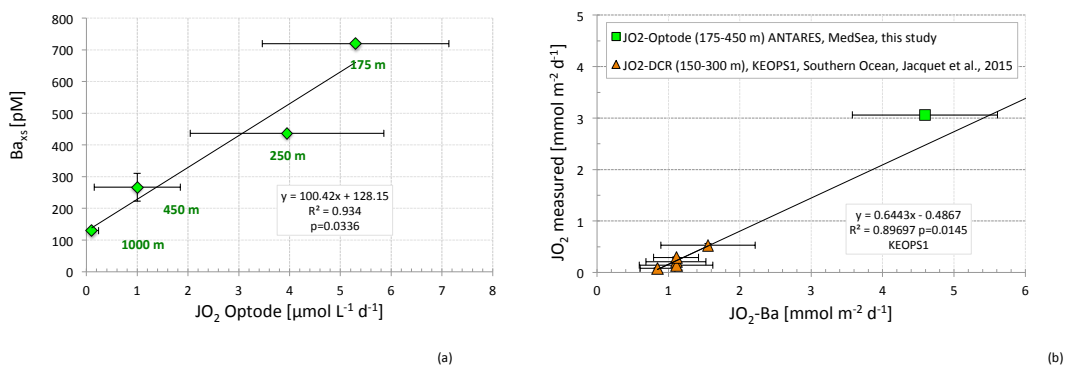
484

485



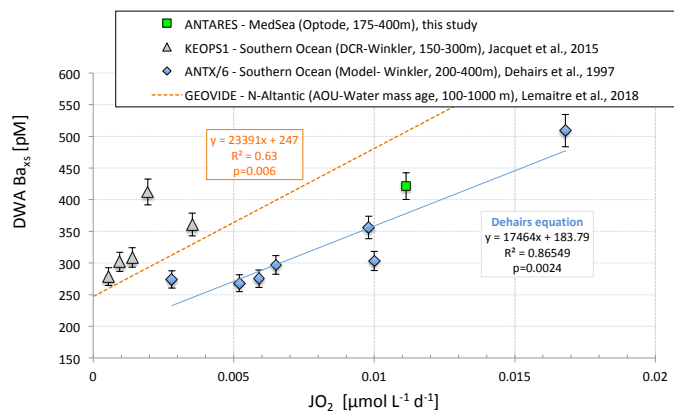
486 FIGURE 3

487



(a)

(b)



(c)

488

489

490